United States
Environmental Protection
Agency

Environmental Sciences Research
Laboratory
Research Triangle Park NC 27711

EPA-600/7-79-088
April 1979

Research and Development

EPA

Surface Reactions of Oxides of Sulfur

Interagency Energy/Environment R&D Program Report

RESEARCH REPORTING SERIES

Research reports of the Office of Research and Development, U.S. Environmental Protection Agency, have been grouped into nine series. These nine broad categories were established to facilitate further development and application of environmental technology. Elimination of traditional grouping was consciously planned to foster technology transfer and a maximum interface in related fields. The nine series are:

1. Environmental Health Effects Research
2. Environmental Protection Technology
3. Ecological Research
4. Environmental Monitoring
5. Socioeconomic Environmental Studies
6. Scientific and Technical Assessment Reports (STAR)
7. Interagency Energy-Environment Research and Development
8. "Special" Reports
9. Miscellaneous Reports

This report has been assigned to the INTERAGENCY ENERGY-ENVIRONMENT RESEARCH AND DEVELOPMENT series. Reports in this series result from the effort funded under the 17-agency Federal Energy/Environment Research and Development Program. These studies relate to EPA's mission to protect the public health and welfare from adverse effects of pollutants associated with energy systems. The goal of the Program is to assure the rapid development of domestic energy supplies in an environmentally-compatible manner by providing the necessary environmental data and control technology. Investigations include analyses of the transport of energy-related pollutants and their health and ecological effects; assessments of, and development of, control technologies for energy systems; and integrated assessments of a wide range of energy-related environmental issues.

This document is available to the public through the National Technical Information Service, Springfield, Virginia 22161.

EPA-600/7-79-088
April 1979

SURFACE REACTIONS OF OXIDES OF SULFUR

by

J. H. Lunsford
Department of Chemistry
Texas A&M University
College Station, Texas 77843

Grant No. R-801136

Project Officer

Jack L. Durham
Atmospheric Chemistry and Physics Division
Environmental Sciences Research Laboratory
Research Triangle Park, North Carolina 27711

ENVIRONMENTAL SCIENCES RESEARCH LABORATORY
OFFICE OF RESEARCH AND DEVELOPMENT
U.S. ENVIRONMENTAL PROTECTION AGENCY
RESEARCH TRIANGLE PARK, NORTH CAROLINA 27711

DISCLAIMER

This report has been reviewed by the Environmental Sciences Research Laboratory, U.S. Environmental Protection Agency, and approved for publication. Approval does not signify that the contents necessarily reflect the views and policies of the U.S. Environmental Protection Agency, nor does mention of trade names or commercial products constitute endorsement or recommendation for use.

ABSTRACT

Surface reactions of several sulfur-containing molecules have been studied in order to understand the mechanism by which sulfate ions are formed on atmospheric aerosols. At 25°C the heterogeneous oxidation of SO_2 by NO_2 to sulfuric acid and sulfate ions occurred on hydrated silica and silica-alumina surfaces. Nitrosonium ions, probably in the form of $NOHSO_4$, underwent surface hydrolysis to form H_2SO_4 and NO. The oxidation of SO_2 by O_2 was undetectably slow on these surfaces; however, the reaction was catalyzed by Mn^{2+} ions in a Y-type zeolite, which is a crystalline aluminosolicate. In this case the only reaction product was a SO_4^{2-} species which was strongly bound in the zeolite micropores. Substantial activity was observed only on partially and fully hydrated zeolites. Molecular oxygen also reacted with H_2S on zeolites and magnesium oxide, but essentially no reactions were observed on silica-alumina. The primary reaction on zeolites resulted in the formation of elemental sulfur; whereas, on MgO a variety of products were observed including elemental sulfur, sulfide ions, sulfite ions and a number of paramagnetic ions such as S_3^-, S_2O^- and S_n^-. Sulfate ions were not formed from H_2S following the reactions at 25°C.

Experiments were also carried out to identify and to determine the mechanism by which S_2O^- and $H_2S_2^-$ ions are formed on MgO. The S_2O^- ion was observed following the surface reaction of H_2S with SO_2, and formation of the ion was promoted by ultraviolet light. A mechanism has been proposed in which S_2 molecules react with oxide ions of the lattice. The $H_2S_2^-$ ion was formed upon reacting H_2S with trapped electrons on the surface. Information on the electronic structure of both paramagnetic species has been obtained from sulfur-33 hyperfine data.

In order to establish the geometric structure of the S_2O^- ion and other paramagnetic sulfur-containing molecules on MgO, CNDO semiempirical calculations were carried out to determine theoretical values of g tensors and spins densities as a function of bond angles and bond length. By comparing the calculated and experimental values, one could establish the structure of the molecule. This represents one of the first attempts to determine the structure of adsorbed paramagnetic ions.

This report was submitted in fulfillment of Grant No. R-801136 by Texas A&M University under the sponsorship of the U.S. Environmental Protection Agency. This report covers the period December 15, 1973 to May 15, 1978 and the work was completed as of November 15, 1978.

CONTENTS

Abstract iii

Figures vi

Tables vii

Acknowledgment viii

1. Introduction 1

2. Experimental 3

3. Results 4

4. Discussion 27

5. List of Publications 30

References 31

FIGURES

Number		Page
1	S(2p) and N(1s) ESCA spectra produced by reacting SO_2 with NO_2.	5
2	Infrared spectra of SO_2 and NO_2 on hydrated SiO_2.	7
3	ESCA spectra of sulfur and manganese 2p levels.	9
4	Initial rate of $SO_4^=$ formation versus SO_2 partial pressure. . .	13
5	XPS spectrum of sulfur 2p lines.	17
6	EPR spectrum of S_2O^- on MgO.	18
7	EPR spectrum of S_2O^- containing sulfur-33 on MgO.	20
8	EPR spectra of $H_2S_2^-$ on MgO.	22
9	EPR spectra of $H_2{}^{33}S_2^-$ on MgO.	23

TABLES

Number		Page
1	Binding Energies (eV) of Adsorbed Species.	4
2	Observed Frequencies of Adsorbed Species.	8
3	Reactive Capacities of MnY Zeolite Catalysts.	10
4	Initial Rates of Reaction.	14
5	g-Values of the Isoelectronic SO_2^-, S_2O^- and S_3^- Ions.	19
6	A Comparison of the Experimental and CNDO/2-Calculated g-Tensors.	25
7	A Comparison of Spin Densities Determined from CNDO/2 Calculations and Experimental Hyperfine Data.	26
8	Spin Density of the Isoelectronic SO_2^-, S_2O^- and S_3^- Ions on MgO.	28

ACKNOWLEDGMENT

The contributions of Dr. Jack L. Durham in keeping the author abrest of current views on the oxidation of SO_2 in the atmosphere was a significant factor in this work. The author also wishes to express appreciation to Prof. R. M. Hedges for the double-precision version of the CNDO/2 program and to Dr. T. T. Yu for assistance in programming.

SECTION 1

INTRODUCTION

Expanding utilization of coal and lignite as primary fuel sources has prompted concern over the fate of sulfur dioxide in the atmosphere. This major pollutant is produced during combustion at a rate in excess of seventy billion pounds per year in the United States (1). In addition, sulfur, mainly in a more reduced state such as found in hydrogen sulfide, is introduced into the atmosphere during the decay of organic matter. Aerosols which contain adsorbed oxides of sulfur have been implicated as causative agents for vegetation damage, reduced visibility, and chronic pulmonary diseases (2,3). For lack of conclusive evidence, the harmful form of sulfur is believed to be the sulfate ion. Of particular importance in this respect are the poorly understood mechanisms through which sulfur dioxide or hydrogen sulfide may be transformed into surface sulfate ions. Potential oxidizing agents include molecular oxygen, ozone, and nitrogen dioxide.

Catalysts for the oxidation of SO_2 have long been known. In 1871, Deacon (4) demonstrated that a solution of $CuSO_4$ was capable of producing sulfuric acid from a gaseous mixture of SO_2 and air. Since that time, solutions of many other salts have been shown to display similar catalytic activity. More recently, several research groups (4-6) have explored the oxidation of SO_2 in water droplets containing dissolved metal salts. The objective of these studies has been to more closely approximate atmospheric conditions by using droplets of a size comparable to those occuring naturally in atmospheric fogs. These studies of SO_2 oxidation have shown that the catalysts in the droplets can display appreciable activity under ideal conditions. Furthermore, the experiment repeatedly indicate that Mn^{2+} is one of the most active catalysts in such systems at ambient temperatures.

No significant results are available regarding the reactivity of adsorbed SO_2 with oxides of nitrogen. This is unfortunate from a practical viewpoint because NO and NO_2 are also common constituents of stack gases, along with SO_2. The related gas phase SO_2-NO_2 reactions have attracted continued interest (7,8). The results generally imply that the photoxidation of SO_2 to SO_3 may occur at high concentration levels; however, at atmospheric levels, which are on the order of 10^{-1}-10^{-2} ppm, quenching by molecular oxygen essentially precludes SO_3 production. Recent evidence (9,10) suggests that photolysis of SO_2-NO_2-air mixtures yields $NOHSO_4$ aerosol which slowly hydrolyzes in air to form sulfuric acid and NO.

It has been suggested that it is possible to obtain sulfate ions from H_2S under ambient conditions, provided a catalyst (an aerosol) is employed. The

oxidation of H_2S by molecular oxygen has indeed been observed, but the major product is elemental sulfur. Moreover, the catalyzed reaction usually requires elevated temperatures and high humidity. Catalysts include activated carbon, molecular sieves, alumina, bauxite and Al-Mg alloy (11-17).

The purpose of this study has been to explore the surface reactions of SO_2 with O_2 (18) and NO_2 (19,20) as well as the reactions of H_2S with O_2 (21). The solids included both acidic alumino-silicates and a basic metal oxide, MgO. Hydrated silica, which is generally considered to be a rather inert solid, was also used during the study with NO_2. The oxidized forms of sulfur were detected both spectroscopically (electron paramagnetic resonance, infrared and X-ray photoelectron spectroscopy) and by wet chemical techniques. In all cases temperatures near ambient were used, although the concentrations of SO_2, H_2S and NO_2 were much higher than those found under atmospheric conditions.

In addition to studying the reactions involving the oxidation of SO_2 or H_2S, research has also been carried out on the formation and structure of paramagnetic sulfur-containing molecules. These molecules include $H_2S_2^-$, which is formed by allowing H_2S to react with trapped electrons on MgO, and S_2O^-, which is formed by reacting H_2S and SO_2 on the same metal oxide (22, 23). In addition to yielding S_2O^-, the reaction between H_2S and SO_2 produces elemental sulfur and water (the Claus reaction). The geometric structure of S_2O^- and other sulfur-containing radicals has been determined by comparing calculated magnetic parameters with those which have been observed experimentally (24).

SECTION 2

EXPERIMENTAL

Details of the experiments may be found in refs. 18-23; however, a summary of the materials and techniques will be described here. Amorphous silica gel and silica-alumina (9.3% alumina) were used as supplied from a commercial source. The BET surface areas of the silica and silica-alumina, obtained from nitrogen adsorption data, were 310 and 360 m^2/g, respectively. The MnY zeolites were obtained by exchanging a sodium form in aqueous solutions of $MnCl_2$ which yielded Mn^{2+} concentrations between 0.4 and 23 ions per unit cell. High surface area magnesium oxide was prepared by reacting reagent grade powder with water at 100°C. The resulting $Mg(OH)_2$ was decomposed under vacuum at 300°C and then 500°C giving MgO which had surface area ca. 200 m^2/g.

With the exception of isotopically enriched SO_2 and H_2S, all of the gases were obtained from commercial sources. Sulfur-33 enriched SO_2 was prepared by allowing 3 mg of sulfur containing 25.5 or 59.2% ^{33}S to react with an excess of pure oxygen at 450°C for 2 hr. Oxygen-17 labeled SO_2 was prepared in a similar manner by using 41.7% enriched $^{17}O_2$. Sulfur-33 enriched H_2S was prepared by allowing 5 mg of sulfur containing 25.5% ^{33}S to react with an excess of pure hydrogen at 300°C for 10 hr. The unreacted gases were removed by the freeze-pump technique prior to adsorption.

The SO_2 uptake and reaction products were determined by gravimetrically measuring the adsorption, by analyzing for the sulfate formed and by several spectroscopic techniques. The sulfate formed in the zeolite was determined by using a barium titration procedure, following the digestion of the zeolite in HCl. The ESCA spectra were obtained on a photoelectron spectrometer using aluminum K_α x-radiation. From the binding energies of the emitted electrons the oxidation state of the sulfur could be determined. Binding energies are referenced relative to the Au $4f_{7/2}$ level (84.0 eV) of gold which was vacuum sputtered onto the samples. Transmission infrared spectra were obtained with the samples in the form of thin self-supporting wafers. The paramagnetic ions were identified by electron paramagnetic resonance (EPR) spectroscopy.

SECTION 3

RESULTS

SURFACE REACTIONS OF SO_2 WITH NO_2

Using ESCA it was determined that SO_2 does not chemisorb on silica or silica-alumina at 25°C, and neither does it react on the surface with O_2 or air. Markedly different behavior was observed when SO_2 and NO_2 were allowed to react at 25°C on the hydrated surfaces. Curve a of Figure 1 was recorded after admitting 25 Torr SO_2 to a silica sample for 4 hr, expanding the excess gas phase to about 2 Torr, and introducing 25 Torr of NO_2 for 4 hr. An intense S(2p) line demonstrates that a strongly bound sulfur oxoanion was formed in the surface reaction. Likewise, curve b illustrates spectra collected from a hydrated $SiO_2 \cdot Al_2O_3$ sample after admitting 8 Torr SO_2 for 20 min, expanding the excess to less than 1 Torr, and subsequently adding 8 Torr NO_2 for 4 additional hr. Both samples were in the spectrometer about 12 hr at 60°C before collecting the N(1s) spectrum, and desorption of the residual species was not detected.

For comparison purposes, curve c depicts the S(2p) and N(1s) ESCA spectrum for $(NH_4)_2SO_4$. The $2p_{3/2}$ and $2p_{1/2}$ binding energies in each spectrum are very close to 168.9 and 169.9 eV, respectively. Based upon the similarity in binding energies following the surface reaction and those observed for $(NH_4)_2SO_4$, we conclude that sulfate ions are present on the surface in both cases. The identification of this and other surface species is given in Table 1.

TABLE 1. BINDING ENERGIES (eV)[a] OF ADSORBED SPECIES

Adsorbate	Orbital	SiO_2	$SiO_2 \cdot Al_2O_3$	Assignment
background	N(1s)	-	401.9(1.9)	NH_4^+
NO_2	N(1s)	407.2(1.8)[b]	407.3(1.8)	NO_3^-
		400.6(1.9)	400.5(1.9)	phys. ads. N_2O_4
$SO_2 + NO_2$	$S(2p_{3/2})$	168.9(1.4)	168.8(1.4)	$SO_4^=$
	$S(2p_{1/2})$	169.9(1.4)	169.9(1.4)	
	S(2s)	233.1(1.9)	233.0(1.9)	
	N(1s)	401.2(1.8)	401.3(1.8)	NO^+ or $-O-\ddot{N}=O$

a) ±0.2 eV
b) (Fwhm)

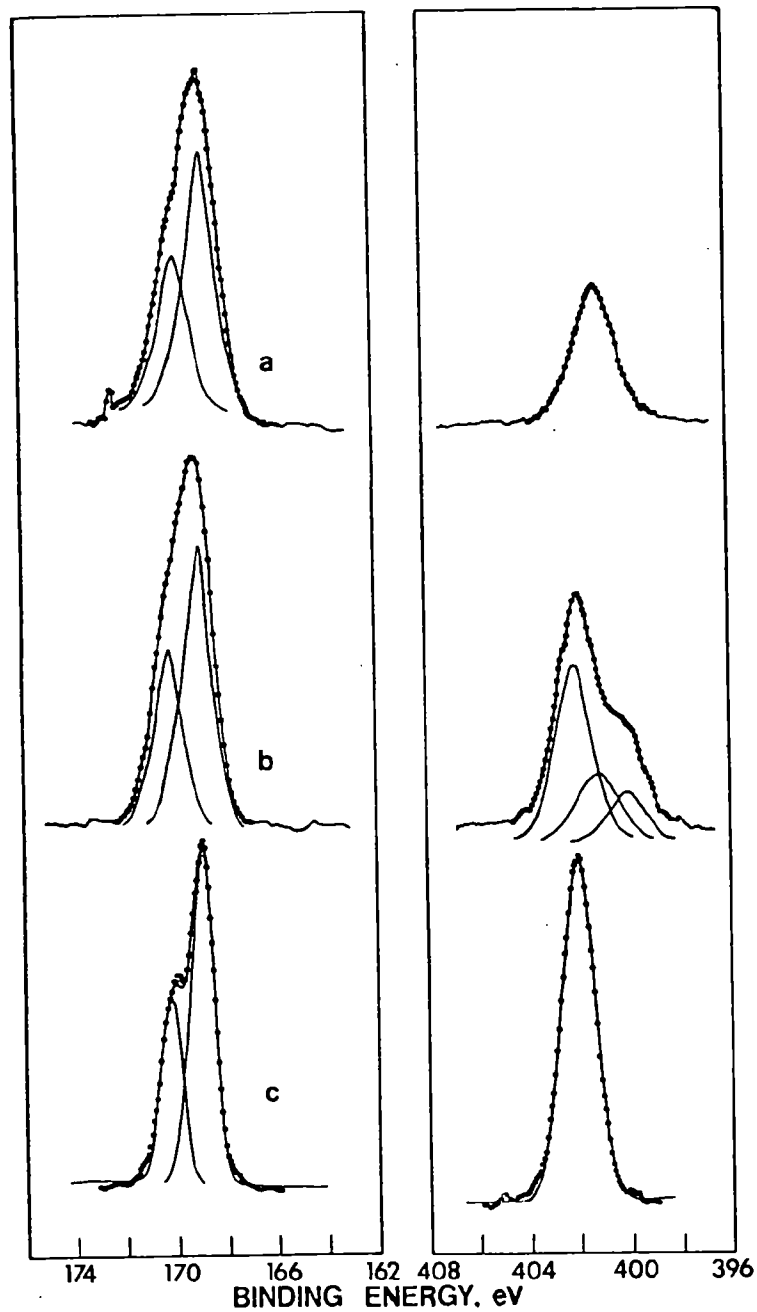

Figure 1. S(2p) and N(1s) ESCA spectra produced by reacting SO_2 with NO_2: (a) SiO_2; (b) $SiO_2 \cdot Al_2O_3$; (c) pure $(NH_4)_2SO_4$.

It should be noted that the formation of NO_3^- was observed when NO_2 alone reacted with the surfaces, but not when NO_2 and SO_2 reacted. The assignment of the N(1s) band at 401.2 eV is made on the basis of both ESCA and infrared data.

Infrared spectra varied with the type of surface and the concentration of adsorbed species. Figure 2 shows the spectra observed for a hydrated silica sample during various stages of adsorption and reaction of SO_2 with NO_2-N_2O_4. The background peak at 1635 cm^{-1}, curve a, is due to adsorption by physisorbed water. Except for windows of relatively low transmission between 500-700 and 900-1000 cm^{-1}, both SiO_2 and $SiO_2 \cdot Al_2O_3$ are infrared opaque below about 1260 cm^{-1}. Curve b shows a low intensity, band at 1337 cm^{-1} due to physically adsorbed SO_2 in equilibrium with gas phase SO_2. Upon further exposure to 7 Torr (solid curves) or 18 Torr NO_2-N_2O_4 (broken curves) in an independent experiment, curve c, bands were produced at 1315 (sh), 1680, 1735 and 2280 cm^{-1}. The band at 1735 cm^{-1} grew slowly in intensity. These peaks, as well as those at 1400 and 2460 cm^{-1} which appeared after degassing 3 hr at 25°C, curved, were all enhanced by higher NO_2-N_2O_4 pressures. The bands at 1400 and 2460 cm^{-1} vanished after readsorbing water vapor (curve e), but both could be restored by further outgassing at 25°C.

These bands, and others observed following the reaction of SO_2 and NO_2 on $SiO_2 \cdot Al_2O_3$ are listed in Table 2 along with the assignments of the vibrational mode responsible for the spectuum. The infrared bands support the formation of a sulfate species; however, a new band at 2460-2465 cm^{-1} suggests that this ion may be present as H_2SO_4 on the surface. Of paramount interest in this work was the mechanism by which SO_2 was oxidized to sulfuric acid on the hydrated surfaces. Dynamic equilibria among adsorbed species are summarized in the scheme below:

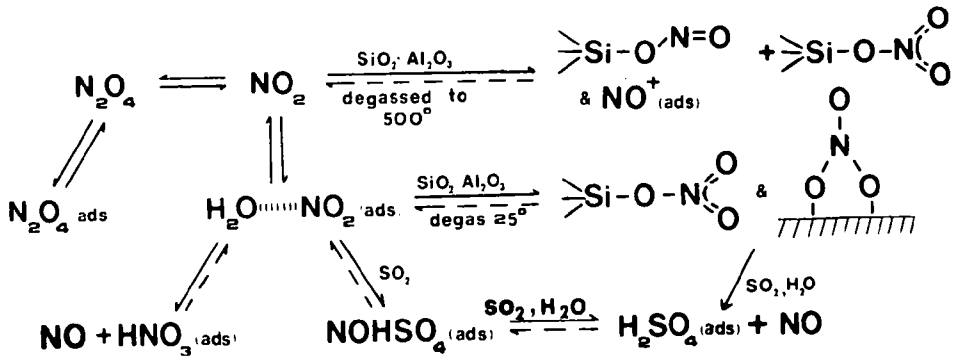

Although not indicated, it should be emphasized that the equilibria generally involve oxidation-reduction reactions and, consequently, may include more than one NO_2 molecule. A nitric acid-like species described earlier was the most reactive of several adsorbed oxides of nitrogen. Reaction with SO_2 is believed to produce $NOHSO_4$. Oxidation probably involves nucleophillic attack of NO_2 upon the coordinatively unsaturated SO_2 molecule. Water, by very rapid or concerted addition to adsorbed SO_2 effects the stabilization of the transition state leading to oxide transfer. The importance of water is born out by the fact that no reaction was detected on dehydrated SiO_2, and different reactions occurred on dehydrated $SiO_2 \cdot Al_2O_3$. Subsequent hydrolysis of nitrosonium bisulfate to form adsorbed sulfuric acid and gas phase NO was facile on SiO_2, slower on $SiO_2 \cdot Al_2O_3$, and irreversible on both surfaces.

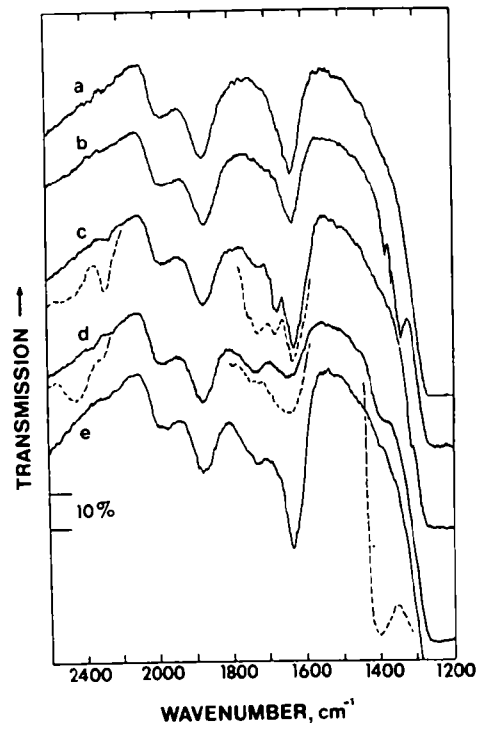

Figure 2. Infrared spectra of SO_2 and NO_2 on hydrated SiO_2: (a) background; (b) 5 Torr SO_2 added 20 min with excess expanded to about 2 Torr; (c) 7 Torr NO_2-N_2O_4 admitted 30 min [(– –) 18 Torr]; (d) degassed at 25°C for 3 hr (6 hr); (e) 8 Torr H_2O adsorbed.

TABLE 2. OBSERVED FREQUENCIES OF ADSORBED SPECIES (cm^{-1})[a]

Adsorbate	SiO_2	$SiO_2 \cdot Al_2O_3$	Assignment
H_2O	1635	1635	υ_2 phys. ads. H_2O
SO_2	1337	1336	υ_3 phys. ads. SO_2
N_2O_4	1735	1730	υ_9-υ(NO) phys. ads. N_2O_4
NO_2	1315(sh)	1320	$\upsilon_2(A_1)$
	1680	1672	$\upsilon_4(B_2)$ $H_2O \cdots N(O)_2$ phys. ads.
	-	690	$\upsilon_3(A_1)$
	1420	1420(sh)	υ_3 NO_3^-
	-	1545	$\upsilon(A_1)$ bidentate nitrato species
	-	1590	υ_{NO_2} antisym. $\geqslant$Si-O-N(O)$_2$
	-	1650[(b)]	$\upsilon_{N=O}$ $\geqslant$Si-O-N=O
$SO_2 + NO_2$	595	610	υ_4 $SO_4^=$
	975	960	υ_1 $SO_4^=$
	2460	2465	υ_{O-H} sym. H_2SO_4
	2280	2270	υ_1 NO^+
	1400	1398	υ_{NO_2} $\geqslant$ Si-O-N(=O)-Si$\leqslant$

sh = shoulder

(a) ± cm^{-1}

(b) only on $SiO_2 \cdot Al_2O_3$ degassed to 500°

SURFACE REACTIONS OF SO_2 WITH O_2

The ESCA spectra of a representative MnY sample, both before and after exposure to the SO_2-O_2 mixture, are shown in Figure 3. The spectrum of pure $MnSO_4$ is included for comparison purposes. From the observed binding energies at 168.8 and 169.9 eV it is evident that sulfate ions were formed in the zeolite during reaction. It also may be noted from the spectra that no other strongly adsorbed sulfur species were present on the catalyst surface either before or after reaction.

Adsorption experiments were undertaken to determine the reactive capacties of the various zeolites. The zeolite samples were allowed 24 hr to react and equilibrate with the reactant gases which contained 40 Torr O_2 and 10 Torr SO_2. To determine quantitatively the fraction of the total irreversible adsorption that was due to the formation of sulfate ions, several samples of MnY used in the adsorption experiments were analyzed for SO_4^{2-} via the barium titration

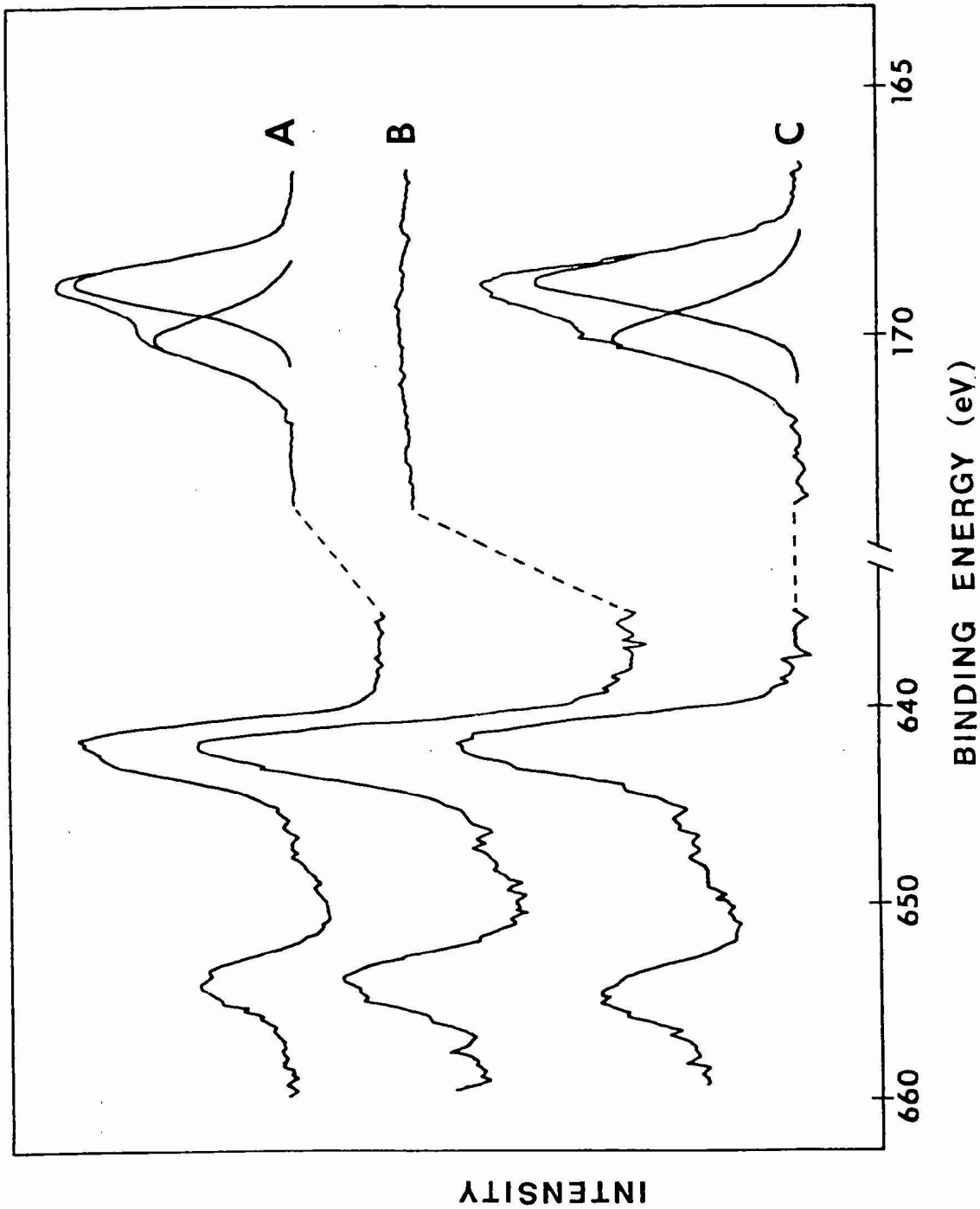

Figure 3. ESCA spectra (contracted scale) of sulfur and manganese 2p levels: (A) reagent $MnSO_4$ reference; (B) MnY zeolite before exposure to SO_2-O_2 reactant gas mixture; (C) MnY zeolite after exposure to reactant mixture of 10 Torr SO_2 and 40 Torr O_2.

technique. It was found in all cases that the irreversibly adsorbed material observed gravimetrically was completely recoverable as SO_4^{2-} using the titration; therefore, the results of the adsorption experiments are reported in Table 3 where all irreversible adsorption has been considered to be due only to the formation of the sulfate ion.

TABLE 3. REACTIVE CAPACITIES OF MnY ZEOLITE CATALYSTS

Manganese concentration (Mn(II)/Unit Cell)	Pretreatment procedure	Irreversible adsorption (no. $SO_4^{=}$ /Unit Cell)	Irreversible adsorption (no. $SO_4^{=}$ /Mn(II))
0.0	Fully Dehydrated	TRACE	-----
0.4	"	1.9	4.7
1.7	"	2.1	1.2
9.0	"	1.6	0.2
16	"	2.2	0.2
0.0	Partially Hydrated	0	0
0.4	"	9.9	24
1.7	"	12.1	7.0
9.0	"	19.0	2.1
16	"	21.2	1.4
0.0	Fully Hydrated	TRACE	-----
0.4	"	45.2	113
1.7	"	50.5	29
9.0	"	46.7	5.1
16	"	49.1	3.2

From these results one may conclude that both the Mn^{2+} ion and O_2 must be present for the oxidation of SO_2 to occur. The formation of SO_4^{2-} was not observed on any of the zeolite samples in the absence of O_2 while only trace amounts of SO_4^{2-} could be detected on NaY in the absence of Mn^{2+}. These trace amounts of SO_4^{2-} could be explained by the presence of iron impurities in the original zeolite.

The reactive capacity of the zeolites was found to be strongly dependent on the degree of dehydration of the MnY catalysts. The amount of SO_4^{2-} formed per unit cell in the fully hydrated samples was more than an order of magnitude greater than the amount formed in the corresponding fully hydrated samples. For any given sample pretreatment, the number of SO_4^{2-} ions formed per unit cell was nearly constant. In contrast, the number of SO_4^{2-} ions produced per Mn^{2+} ion was highly variable and reached its maximum value of 113 for the fully hydrated MnY sample containing 0.4 Mn^{2+} ions per unit cell. This large turnover simply demonstrates that the reaction was catalytic with respect to manganese.

The above observations show that water in the zeolite strongly affects the reaction. It is possible that water functions as a reactant according to the following scheme:

$$SO_{2(g)} \rightarrow SO_{2(adsorbed)} \quad (1)$$

$$SO_{2(adsorbed)} + \tfrac{1}{2}O_2 \rightarrow SO_3 \quad (2)$$

$$SO_3 + H_2O \rightarrow H_2SO_4 \quad (3)$$

This production of sulfuric acid would be expected to make the catalyst more acidic. Since the catalytic oxidation of SO_2 by some solutions of Mn(II) salts is known to have pH limitations (27), it is possible that the reaction within the zeolite micropores is likewise pH limited. As an alternative, SO_3 may react with lattice oxide ions

$$SO_3 + O^{2-}{}_{(lattice)} \rightarrow SO_4^{2-}{}_{(adsorbed)} \quad (4)$$

and water may simply provide a transport mechanism for the migration of SO_4^{2-} ions away from the active sites within the zeolite.

The crystallinity of the zeolite during reaction comes under question since the above mechanisms involve the participation of lattice oxide ions and the production of sulfuric acid. The x-ray powder diffraction patterns of the catalysts indeed were modified after the reaction occurred. There was a decrease in the intensity of some of the reflections while the background level remained reasonably constant. It is not known at this time whether (a) the crystal lattice was partially disrupted as a result of the reaction or (b) the changes in the pattern were simply a result of the added electron density in the interior of the catalyst due to the production of large amounts of sulfate product. This matter is presently under investigation.

Initial rate experiments were conducted using partially hydrated MnY zeolite to determine the reaction rate dependence, if any, on the concentrations

of SO_2, O_2 and Mn^{2+}. Initial rate studies were not conducted on the fully hydrated and fully dehydrated MnY sample because in the former case the rate of adsorption of the reactant gases was extremely slow due to occlusion of the micropores by water molecules, and in the latter case only small amounts of SO_4^{2-} ions could be formed, which led to a relatively large experimental error.

The results of the rate study are presented in Table 4 and in Figure 4. There is an apparant first order rate dependence which is best described in Figure 4 by the linear rate dependence on the pressure of SO_2. Table 4A demonstrates that the reaction was independent of total pressure as was found by increasing the total pressure in the system with helium. Furthermore, Tables 4B and 4D show that the initial rates of reaction were independent of O_2 pressure and temperature respectively.

It is recognized that the observed kinetics in such heterogeneous reactions on porous catalysts may not be representative of the true reaction kinetics if there are diffusion processes in action which can influence the rate of reaction. The fact that the initial rate did not significantly increase as the temperature was raised from 5^oC to 60 C is an indication that diffusion indeed may be limiting the overall reaction. Further evidence that the reaction is diffusion limited may be found in the fact that the reaction rate increased significantly upon addition of small amounts of Mn^{2+} to the zeolite, but additional exchange of Mn^{+} resulted in only modest rate enhancement as shown in Table 4C.

Of the three various types of diffusional limitations, only Knudsen diffusion fits the experimental observations. The Knudsen diffusion coefficient is independent of total pressure, P, while the rates of bulk diffusion and diffusion across a static film are inversely proportional to $\sqrt{P}$. That Knudsen diffusion is operative in this system is not surprising since the conditions for Knudsen flow is that λ, the mean free path of a gas molecule be much larger than the micropore radius. The value of λ is given approximately by

$$\lambda \simeq \frac{7 \times 10^{-3}}{P(\text{Torr})} \text{ cm} \qquad (5)$$

which is on the order of 10^{-4} cm in this system. Obviously, this is considerably larger than the micropore radius of 8×10^{-8} cm in the Y zeolite.

Under conditions of Knudsen diffusion the pseudo-order of the initial rate of reaction with respect to SO_2 pressure may be found from the equation:

$$\text{Observed Order} = (n + 1)/2 \qquad (6)$$

where n is the true reaction order. Thus, it is postulated that the oxidation of SO_2 on MnY catalysts would be a first order process in the absence of the Knudsen diffusion limitation. This result is reassuring since it agrees with the findings of many other authors, most notably Cheng et al. (6), who have studied other heterogeneous catalysts containing maganese.

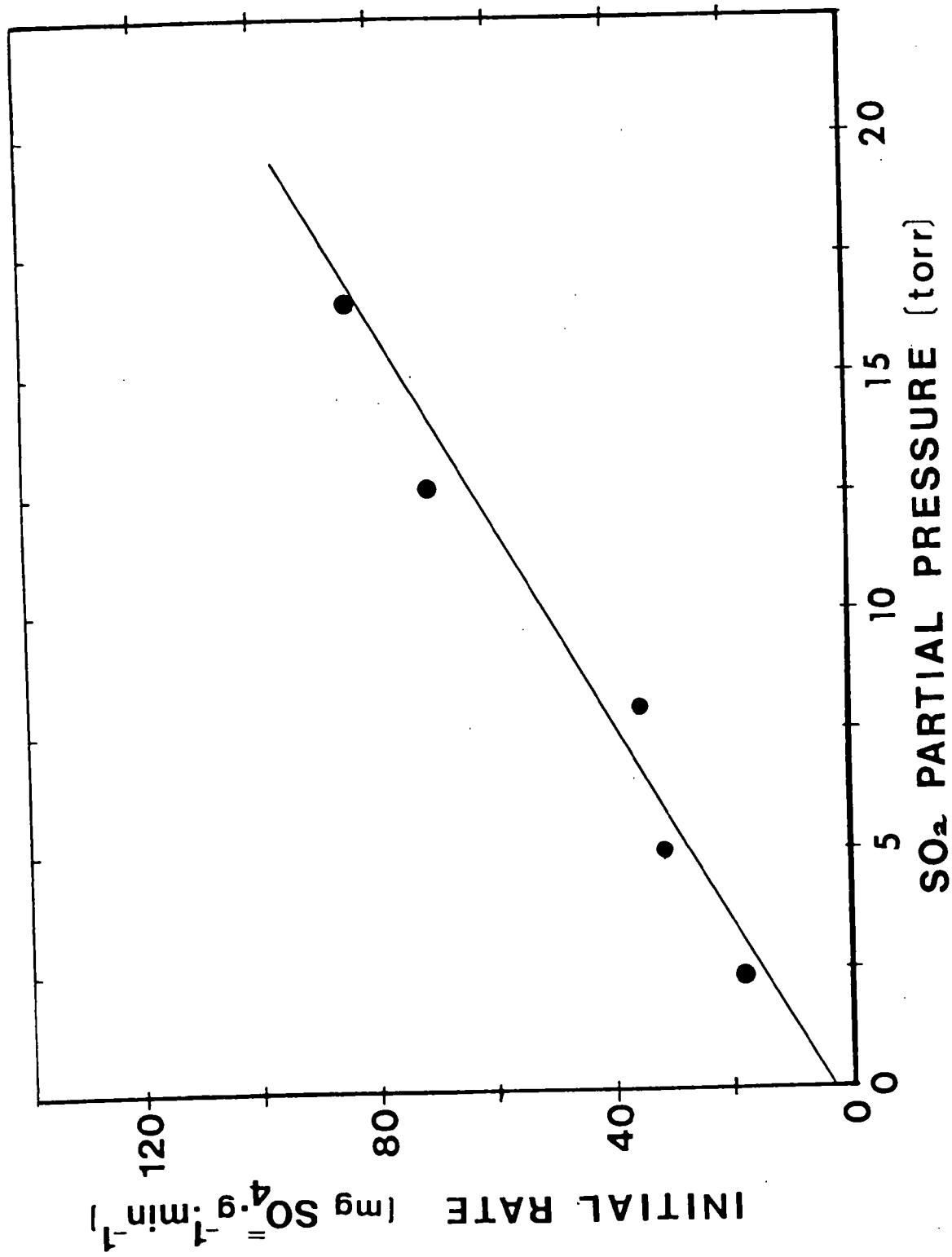

Figure 4. Initial rate of $SO_4^=$ formation versus SO_2 partial pressure.

TABLE 4. INITIAL RATES OF REACTION

A. Initial rate as functions of SO_2 pressure and total pressure

Manganese concentration (Mn(II)/Unit Cell)	Reaction temperature (°C)	P_{SO_2} (Torr)	P_{O_2} (Torr)	P_{He} (Torr)	Initial rate (mg $SO_4^{=}$ g catalyst^{-1} min^{-1})
20.2	25	2.5	20	27.5	19.3
20.2	25	5.0	20	25	31.1
20.2	25	8.0	20	22	37.5
20.2	25	13	20	17	71.6
20.2	25	17	20	13	84.2
20.2	25	17	20	63	83.6
20.2	25	17	20	163	85.2

B. Initial rate as function of O_2 pressure

Manganese concentration (Mn(II)/Unit Cell)	Reaction temperature (°C)	P_{SO_2} (Torr)	P_{O_2} (Torr)	P_{He} (Torr)	Initial rate (mg $SO_4^{=}$ g catalyst^{-1} min^{-1})
20.2	25	10	40	0	97
20.2	25	10	25	15	103
20.2	25	10	20	20	116
20.2	25	10	10	30	101
20.2	25	10	5	35	96

(continued)

TABLE 4 (cont.)

C. Initial rate as function of manganese concentration

Manganese concentration (Mn(II)/Unit Cell)	Reaction temperature (°C)	P_{SO_2} (Torr)	P_{O_2} (Torr)	Initial rate (mg $SO_4^{=}$ g catalyst^{-1} min^{-1})
0	25	7.5	24	0
0.4	25	7.5	24	26.2
1.7	25	7.5	24	29.0
9	25	7.5	24	35.8
16	25	7.5	24	39.1
23	25	7.5	24	40.9

D. Initial rate as function of temperature

Manganese concentration (Mn(II)/Unit Cell)	Reaction temperature (°C)	P_{SO_2} (Torr)	P_{O_2} (Torr)	Initial rate (mg $SO_4^{=}$ g catalyst^{-1} min^{-1})
16	60	10	40	56
16	50	10	40	55
16	40	10	40	59
16	30	10	40	47
16	20	10	40	47
16	10	10	40	59
16	5	10	40	54

SURFACE REACTIONS OF H_2S WITH O_2

The ESCA spectrum of a MnY zeolite after the introduction of H_2S and O_2 showed only one sulfur species which is assigned to elemental sulfur by its $2p_{3/2}$ and $2p_{1/2}$ binding energies of 162.8 and 164.0, respectively. A spectrum of sulfur, however of much lower intensity, was obtained without the exposure of the sample to oxygen. The elemental sulfur remained on the surface after it had been exposed to the atmosphere for 2 weeks. On NaY a similar spectrum was observed after the reaction, although the concentration of elemental sulfur was less than half as great as with the MnY zeolite. The dissociation of H_2S over zeolites to form elemental sulfur has been previously studied, and the results reported here further demonstrate that no higher oxidation states of sulfur are formed. On amorphous silica-alumina virtually no sulfur lines were present in the ESCA spectrum.

The ESCA spectrum of the dehydrated MgO, after it had been treated with H_2S, followed by a 3 min exposure to air during the transfer of the sample to the spectrometer, indicated the formation of two sulfur species; elemental sulfur and sulfide ions (Figure 5A). Brief exposure to the atmosphere showed no evidence of further oxidation; however, when the H_2S-treated MgO was purposely exposed to pure oxygen, the ESCA spectrum indicated an additional peak (Figure 5b). Deconvolution of the spectrum suggested the sulfur $2p_{3/2}$ maxima at 167.0, 162.9 and 160.8 eV, which are in good agreement with the binding energies of sulfites, elemental sulfur and sulfides, respectively. The formation of sulfite ions was favored by low coverage of H_2S and by long exposure of the sample in air, which is evident in Figure 5c. This sample of MgO was first exposed to H_2S and O_2, and then to the atmosphere for 2 weeks. On a hydrated $MgO/Mg(OH)_2$ surface similar results were obtained; however, the sulfur bands were much less intense. The fractional monolayer coverage of the sulfite ions formed on MgO varied from 0.1 to 0.8, depending on the equilibrium pressure of the H_2S and the duration of exposure in air.

Upon freezing the H_2S and O_2 above the dehydrated MgO which was at -196°C a small amount of SO_3^- was evident in the EPR spectrum with g = 2.0034. Upon warming to 25°C for 5 min the catalyst turned yellow and the spectrum of SO_3^- disappeared. A much greater concentration of S_2O^-, which is characterized by g_1 = 2.030, g_2 = 2.010 and g_3 = 2.001 was observed. Moreover, the EPR spectrum recorded at -196°C indicated the formation of the S_3^- ion, which is characterized by $g_\perp$ = 2.043 and $g_{||}$ = 2.004. A relatively small peak at g = 2.052 was observed at both 25°C and -196°C, in addition to the spectrum of S_2O^- and S_3^-, following the oxidation of H_2S by O_2. This species dominated the spectrum at higher coverages of H_2S, and the g values (g_1 = 2.052, g_2 = 2.033, g_3 = 2.002) correspond well with those assigned to S_n^-. No EPR signals were detected for sulfur species on zeolites or on silica-alumina.

ELECTRON PARAMAGNETIC RESONANCE EVIDENCE FOR THE FORMATION OF S_2O^- ON MgO

Hydrogen sulfide and sulfur dioxide react on many types of surfaces, forming elemental sulfur and water (the Claus reaction). In addition, on MgO a paramagnetic ion identified as S_2O^- was also formed. This ion exhibited the spectrum shown in Figure 6 with the indicated g values. Four hyperfine lines with a splitting of 47.6G, centered on g_{xx}, were observed when SO_2 enriched to 25.5% ^{33}S was used (Figure 7a). When H_2S enriched to 25.5% ^{33}S was

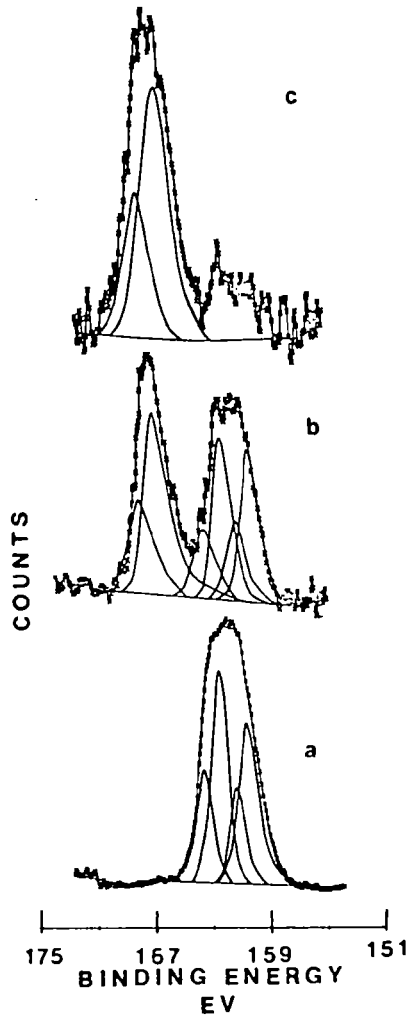

Figure 5. XPS spectrum of sulfur 2p lines, formed on MgO after the adsorption of (a) H_2S, (b) H_2S and O_2 and (c) H_2S and O_2, in atmosphere for 2 weeks, at 25°C.

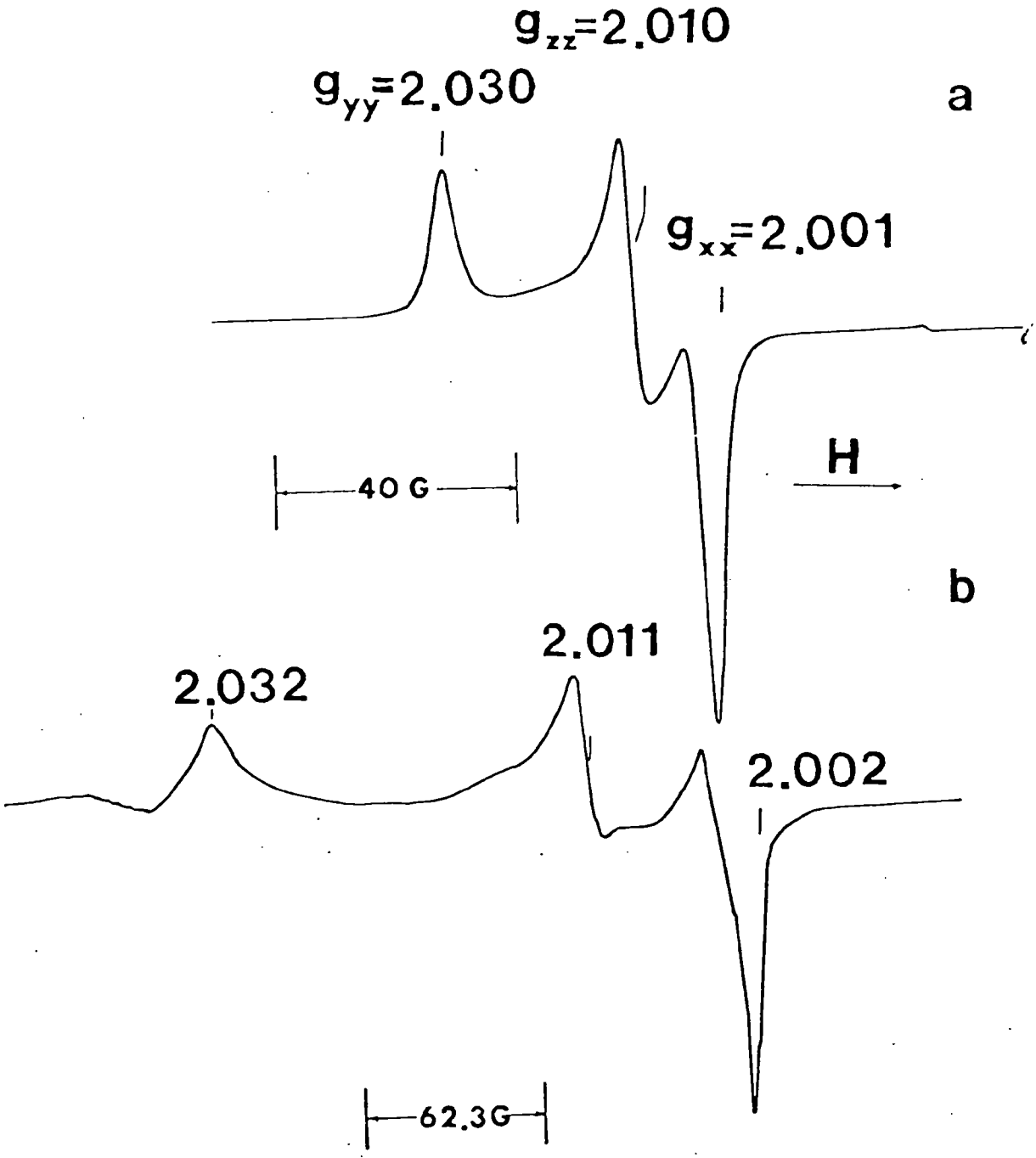

Figure 6. EPR spectrum of S_2O^- formed by allowing H_2S and SO_2 to react on magnesium oxide at room temperature, followed by irradiation at 254 nm: (a) X-band, (b) Q-band.

employed, another set of four hyperfine lines with a splitting of 32.6G, also centered on g_{xx}, was detected as shown in Figure 7b. Both sets of hyperfine lines of approximately equal intensity were observed as the result of the reaction of H_2S with enriched SO_2 which contained 59.2% ^{33}S. Hyperfine structure resulting from the adsorption of SO_2 enriched to 41.7% in ^{17}O was not observed. No change in the EPR spectrum was detected when D_2S was used instead of H_2S.

From the ^{33}S (I=3/2) hyperfine splitting observed it is evident that two sets of four lines result from two nonequivalent ^{33}S atoms. Although some isotope mixing occurred during the formation of the paramagnetic ion, the results suggest that the hyperfine splitting of 48.6G was mainly due to the ^{33}S which originated from SO_2; whereas, the splitting of 32.6 was mainly due to the ^{33}S which originated from H_2S. The mixing was more apparent in the spectrum of the more highly enriched (59.2% ^{33}S) SO_2.

Morton (25) originally based the assignment of the S_2O^- ion on a comparison of trends in principal g values for the ions SO_2^-, S_2O^-, and S_3^- where the effect of the larger spin orbit coupling becomes increasingly greater with more sulfur atoms in the molecule. Since oribitals available for mixing with the ground state are rather far removed in energy, the effect of local environment is small, and the spectra are reasonably independent of the particular matrix or surface. This is evident, for example, when one compares the g values of SO_2^- on S_3^- on surfaces and irradiated crystals, as shown in Table 5.

TABLE 5. g-VALUES OF THE ISOELECTRONIC SO_2^-, S_2O^- AND S_3^-

	g_1	g_2	g_3	ref.
SO_2^-/MgO (A)	2.0097	2.0052	2.0028	26
(B)	2.0078	2.0033	2.0014	26
SO_2^-/Zeolites	2.002	2.002	2.009	27
SO_2^-/KCl	2.0100	2.0071	2.0025	28
S_2O^-/MgO	2.030	2.010	2.001	this work
S_2O^-/Sodalite	2.029	2.011	2.001	29
$S_2O^-/Na_2S_2O_3 \cdot 5H_2O$	2.0287	2.0106	2.0035	25
S_3^-/MgO	2.043	2.043	2.004	30
S_3^-/Sodalite	2.046	2.036	2.005	29
S_3^-/KCl	2.0499	2.0319	2.0026	28

The absence of any oxygen hyperfine splitting is somewhat difficult to understand since ^{17}O has a rather large nuclear magnetic moment, and even a spin density as low as 0.05 would result in a separation of approximately 25G between terminal hyperfine lines. It seems more reasonable that the oxygen in

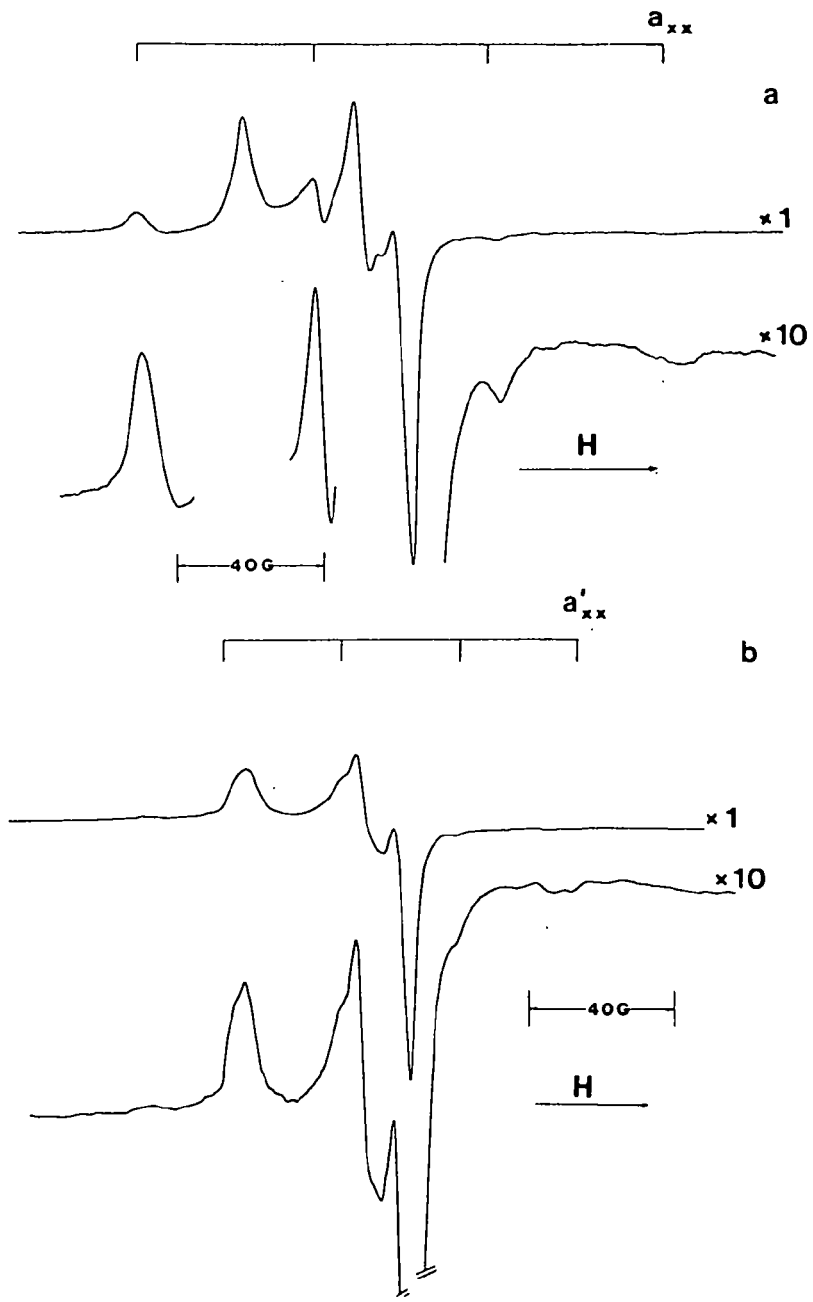

Figure 7. EPR spectrum of S_2O^- formed by allowing (a) H_2S to react with 25.5% ^{33}S-enriched SO_2, (b) 25.5% ^{33}S-enriched H_2S to react with SO_2 on MgO.

S_2O^- is derived from the oxide ions of the lattice, rather than from the SO_2. Furthermore, justification for this model comes from the observation that S_2O^- could be formed by irradiation of CS_2 or COS adsorbed on MgO. We suggest that sulfur molecules (S_2, S_3,...S_n) are deposited on the surface of MgO by the reaction of H_2S with SO_2 and by irradiation of adsorbed COS or CS_2. The subsequent reactions

$$S_2 + O^{2-}(MgO) \xrightarrow[h\nu]{} S_2O^- + e^- \quad (7)$$

and

$$S_3 + e^- \xrightarrow[h\nu]{} S_3^- \quad (8)$$

yield the observed paramagnetic ions. It is likely that S_2^- was also formed, but the EPR spectrum was not observed at -196°C because of a short spin relaxation time. The partial pressures of H_2S and SO_2 over the MgO may affect the distribution of molecular weights of the sulfur species, and thereby alter the concentration of S_2O^-. The role of oxide ions is further substantiated by the absence of S_2O^- on MgO-$Mg(OH)_2$ where the surface is covered with hydroxide ions.

ELECTRON PARAMAGNETIC RESONANCE EVIDENCE FOR THE FORMATION OF $H_2S_2^-$ ON MgO

Trapped electrons (S centers) may be produced by irradiating MgO in the presence of hydrogen with a 254-nm ultraviolet lamp. Upon warming a sample tube containing frozen H_2S and MgO with S centers to -78°C the EPR spectrum shown in Figure 8a was observed. This spectrum can best be understood in terms of two forms of $H_2S_2^-$. One form (A) is characterized by $g_\perp$ (A)=2.015 and $g_\parallel$ (A)=2.003 with two nonequivalent protons having $a_\perp{}^H(A) = a_\parallel{}^H(A)$=9.4G and $a_\perp{}^{H'}(A) = a_\parallel{}^{H'}(A)$ = 6.6G. The other form (B) is isotopic and is characterized by $g_{iso}(B)$ = 2.009 with $A_{iso}{}^H(B)$ = 9.4G and $a_{iso}{}^{H'}(B)$ = 6.6G. The simulated spectrum using these parameters and a concentration ratio of A/B = 5.7 is given in Figure 8b.

The relative intensities of A and B may be altered by changing the mode of formation. When the sample was irradiated at -196°C following the adsorption of H_2S on S centers, the color of the sample became yellow and species A dominated the spectrum. The hydrogen hyperfine lines in the parallel direction became more evident, although some of the isotropic spectrum was still observed. Upon warming the sample to 25°C the color changed to white and no paramagnetic species was observed.

When H_2S enriched to 25.5% in sulfur -33 was adsorbed on MgO containing S centers, the EPR spectrum revealed additional hyperfine lines as depicted in Figure 9A. Upon irradiation at 254 nm for 10 min the relative intensity of species B was greatly reduced; whereas, two sets of quartet lines having splitting constants 61 and 41 G, centered on $g_\parallel$ of species A became apparent. These additional hyperfine lines were much more obvious when H_2S enriched to 59.2% in sulfur - 33 was used. Using the statistical isotope distributions for 25.5% ^{33}S the spectrum of Figure 9b was simulated for the g values and hydrogen hyperfine splitting indicated previously, and with $|a_\perp{}^s(A)| = |a_\perp{}^{s'}(A)|$ = 2G, $|a_\parallel{}^s(A)|$ = 61G, $|a_\parallel{}^{s'}(A)|$ = 41G, $|a_{iso}{}^s(B)|$ = 13G, $|a_{iso}{}^{s'}(B)|$ =9G, and a concentration ratio of A/B = 5.7.

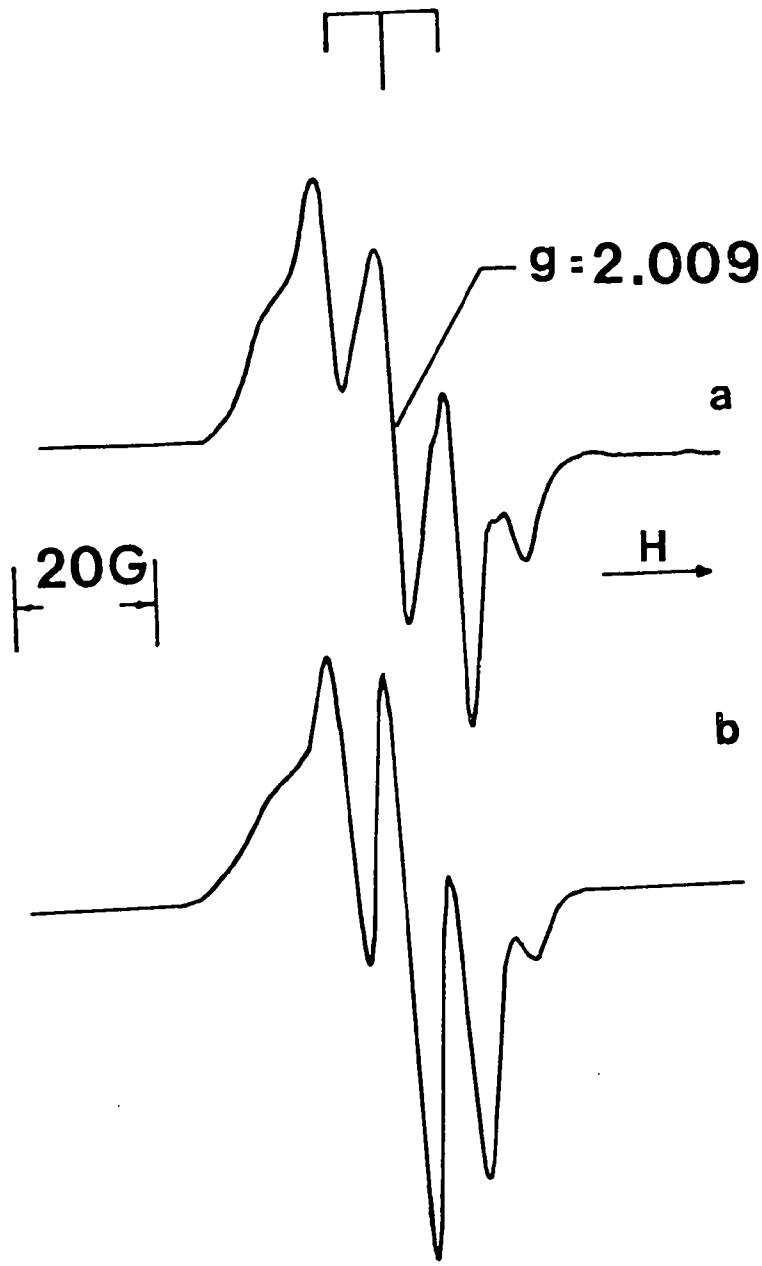

Figure 8. EPR spectra of $H_2S_2^-$ obtained by allowing H_2S to react with trapped electrons on MgO at -78°C: (a) experimental spectrum; (b) simulated spectrum using a mixing ratio A/B = 5.7.

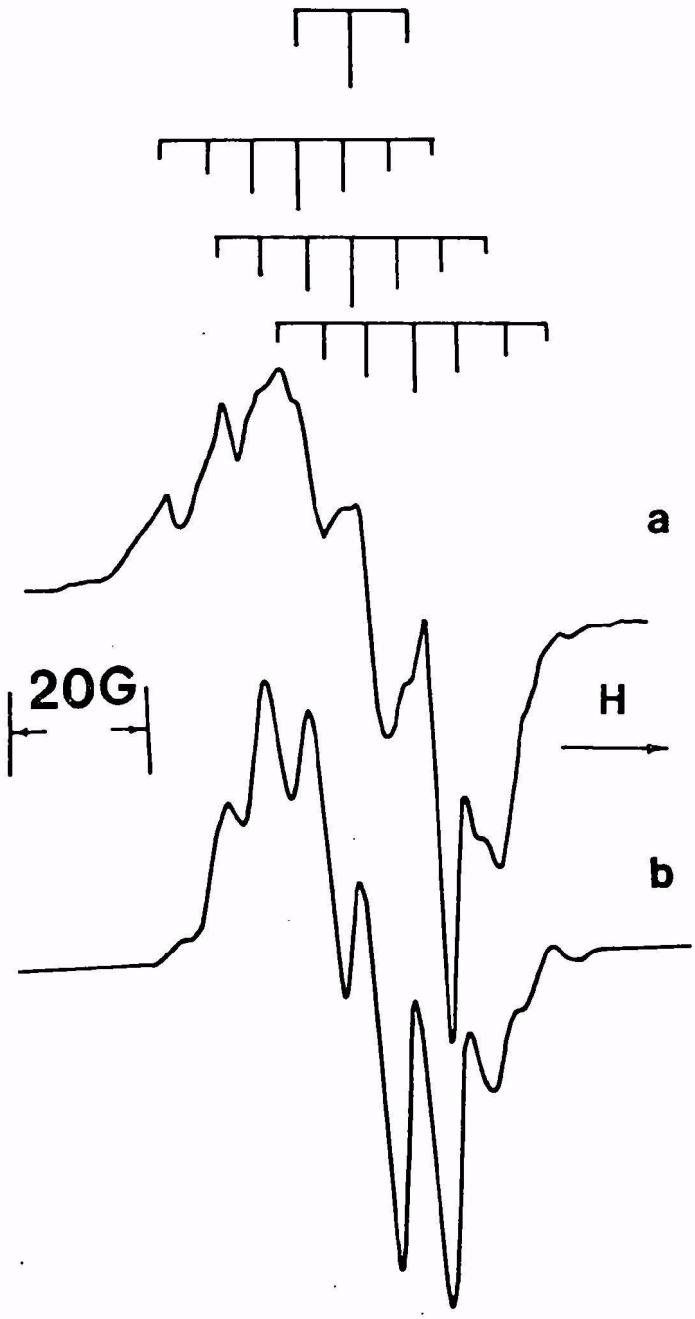

Figure 9. EPR spectra of $H_2{}^{33}S_2^-$(B) obtained by allowing 25.5% ^{33}S-enriched H_2S to react with trapped electrons on MgO at -78°C: (a) experimental spectrum; (b) simulated spectrum.

The g values obtained for species A are in reasonably good agreement with those reported by Bennett et al. (31) for the spectrum assigned to the H_2S^- radical. We believe, however, that the hyperfine structure is derived from two nonequivalent hydrogen atoms and two nonequivalent sulfur atoms for species A, and perhaps species B. The situation is not so clear with respect to species B since there is overlapping of hyperfine lines in the EPR spectrum. Better agreement between the experimental and simulated spectra was obtained using the model $H_2S_2^-$, rather than H_2S^-. It is proposed that the isotropic spectrum is the result of ion motion on the surface in three dimensions.

The mode of formation of the radicals via the transfer of electrons from the surface to the adsorbed H_2S confirms that the observed species are anions. When H_2S is adsorbed on the S^- centers of MgO, the H_2S^- ion may be formed initially. This ion may then react with a neutral H_2S molecule, forming $H_2S_2^-$ and H_2. Subsequent irradiation undoubtedly leads to the photolysis of H_2S and other reactions which may result in additional $H_2S_2^-$ and elemental sulfur. The nonequivalency of the two sulfur and two hydrogen atoms may be due to the effect of the surface environment. The reason for the high mobility experienced by part of the $H_2S_2^-$ molecules is not understood at this time.

CALCULATIONS OF THE g TENSORS AND SPIN DENSITIES OF SMALL PARAMAGNETIC SULFUR-CONTAINING ANIONS ON MAGNESIUM OXIDE

Using a CNDO semiempirical calculation principal values of g tensors and spin densities have been determined for the sulfur-containing molecules SO_2^-, SSO^-, S_3^-, SCO^-, and CS_2^-, as well as CO_2^-. A deviation Δ is defined as the average of the absolute deviation between the principal values of the experimental and the calculated g tensors: $\Delta = \frac{1}{3}(|\Delta_{x'}| + |\Delta_{y'}| + |\Delta_{z'}|)$. In the course of minimizing Δ, we started with the bond length suggested for the neutral molecule, and the bond angles were varied between 90 and 150°. By plotting Δ versus bond angle a curve with a minimum was generally obtained. By varying both the bond length and bond angle within reasonable values a true minimum, which corresponds to the most likely molecular structure of the ion on the surface of MgO was found. These calculate g tensors that correspond to the minimum Δ values are tabulated in Table 6. The calculated g values were often within experimental error.

The calculations also yielded spin densities which are compared with the experimental values in Table 7. The spin densities of the sulfur and oxygen atoms are generally consistent with the experimental finding; however, the spin densities in the p orbital of the central sulfur atoms are usually lower by 7 to 16% than the experimental values. The difference is reasonable since the estimates based on hyperfine data were obtained by neglecting the d-orbital contribution. Nevertheless, the theoretical calculations indicate that the contribution of sulfur d orbitals is only 3 to 11%.

TABLE 6. A COMPARISON OF THE EXPERIMENTAL AND CNDO/2-CALCULATED g-TENSORS

MOLECULE	BOND LENGTH Å	BOND ANGLE °	EXPERIMENTAL				CNDO/2			
			$^*g_{iso}$	g_{xx}	g_{yy}	g_{zz}	g_{iso}	g_{xx}	g_{yy}	g_{zz}
SO_2^-(A)	S-O 1.560	120	2.0059	2.0097	2.0052	2.0028	2.0058	2.0097	2.0057	2.0021
SO_2^-(B)	S-O 1.500	110	2.0042	2.0078	2.0033	2.0014	2.0043	2.0075	2.0033	2.0021
SSO^-	S-O 1.560 S-S 2.100	120	2.014	2.030	2.010	2.003	2.0151	2.0287	2.0144	2.0021
S_3^-	S-S 2.100	110	2.030	2.043	2.043	2.004	2.0304	2.0452	2.0439	2.0022
CO_2^-	C-O 1.060	121	2.0007	2.0032	1.9975	2.0014	2.0010	2.0032	1.9975	2.0023
SCO^-	C-O 1.159 C-S 1.653	113	1.9977	2.0049	1.986	2.0022	1.9973	2.0049	1.9858	2.0012
CS_2^-	C-S 1.850	130	1.9902	1.9999	1.963	2.0078	1.9885	1.9991	1.9653	2.0012

$^*g_{iso} = g_{isotropic}$

TABLE 7. A COMPARISON OF SPIN DENSITIES DETERMINED FROM CNDO/2 CALCULATIONS AND EXPERIMENTAL HYPERFINE DATA

MOLECULE / ORBITAL	SO_2^-(A)		SO_2^-(B)		SSO^-		S_3^-		CO_2^-		SCO^-		CS_2^-	
	Exptl[a]	CNDO	Exptl	CNDO	Exptl	CNDO	Exptl	CNDO	Exptl	CNDO	Exptl	CNDO	Exptl	CNDO
C s	-		-		-		-		0.18	0.18	NA[b]	0.11	NA[b]	0.08
C p_z	-		-		-		-		0.45	0.34		0.20		0.34
O p_{z1}	0.14	0.15	0.12	0.12	0.07[c]	0.08	-		0.20	0.24		0.19		-
O p_{z2}	0.14	0.15	0.12	0.12	-		-		0.20	0.24	(O p_y	0.05)		-
S^o s^d	0.01	0.00	0.01	0.00	0.02	0.00	0.01	0.00	-			0.00		0.00
S^o p_z^d	0.75	0.64	0.71	0.64	0.54	0.45	0.53	0.37	-			-		-
S p_{z1}	-		-		0.37	0.43	0.27	0.30	-			0.26		0.24
S p_{z2}	-		-		-		0.27	0.30	-		(S p_y	0.16)		0.24
d-orbital contribution		0.07		0.11		0.05		0.03		0.00		0.03		0.08

[a]Calculated from experimental hyperfine data

[b]Not available

[c]Spin density estimated by difference from unity

[d]Central sulfur atom

SECTION 4

DISCUSSION

The results presented here confirm that a variety of reactions involving sulfur-containing molecules can occur on solid surfaces. Nitrogen dioxide is an active molecule for the oxidation of sulfur dioxide to adsorbed sulfuric acid on hydrated silica and silica-alumina at 25°C. Although direct proof for $NOHSO_4$ as an intermediate is lacking, the experimental evidence strongly favors this interpretation. Nitrosonium bisulfate is an important intermediate in the gas phase oxidation of SO_2 to H_2SO_4 with NO_2 and water at high pressures and temperatures; e.g., the lead chamber process incorporates this reaction. In the chamber process the reaction,

$$2NOHSO_4 + 2H_2O + SO_2 \rightarrow 3H_2SO_4 + 2NO \qquad (9)$$

is postulated, and a similar reaction apparently takes place on the surface of silica and silica-alumina. Similar reactions may occur among air pollutants on the surfaces of particulates suspended in the atmosphere. It remains to be demonstrated, however, that the rate of reaction will be significant at the lower concentrations of NO_2 and SO_2 that are found under most atmospheric conditions.

In contrast to nitrogen dioxide, it is not possible to oxidize sulfur dioxide using molecular oxygen on the same silica or silica-alumina surfaces at ambient temperatures. The latter reaction did occur on a crystalline aluminosilicate, known as a zeolite, which contained manganese ions. The reaction was catalytic in that up to 113 sulfate ions were formed per manganese ion. The maximum amount of sulfate ion was about 48 per unit cell or 7 per large cavity. This maximum is probably not due to geometric constraints; more likely, it results from the availability of lattice oxygen ions for sulfate formation, assuming that reaction 4 is correct. Since the reaction was diffusion controlled, the inherent rate of reaction is much greater than was observed in these experiments. Although the concentration of exchange sites is more limited, in principle similar reactions should occur on amorphous silica-alumina containing manganese, or perhaps other transition metal ions as impurities.

The surface oxidation of hydrogen sulfide also occurs at moderate temperatures, but the products are elemental sulfur and sulfite ions on magnesium oxide. In addition, small concentractions of the paramagnetic ions S_3^-, S_2O^-, SO_2^-, SO_3^-, and S_n^- were also observed on the surface of MgO during the various stages of the oxidation reaction. The oxidation of H_2S by O_2 at 25°C was different on the three materials: MgO, zeolites and amorphous silica-alumina.

The oxidation was carried out to the greatest extent (sulfite ions) on the basic MgO surface; whereas, it proceeded to form elemental sulfur on zeolites, and was negligibly slow on the acidic silica-alumina surface. The Mn^{2+} ions in the zeolite enhanced the formation of elemental sulfur. There was no evidence for the formation of sulfate ions on any of these surfaces; thus, it appears unlikely that natural sources of H_2S in the environment would contribute significantly to the formation of sulfate ions.

In the process of the reaction between H_2S and SO_2 on MgO paramagnetic S_2O^- ions were produced, in addition to elemental sulfur and water. The ^{33}S hyperfine structure observed in these experiments confirms the previous identification of the ion by EPR spectroscopy. The spin densities of S_2O^- and the isoelectronic SO_2^- and S_3^- ions are compared in Table 8. The variations

TABLE 8. SPIN DENSITY OF THE ISOELECTRONIC SO_2^-, S_2O^- and S_3^- ON MgO

	SO_2^-(A)	SO_2^-(B)	S_2O^-	S_3^-
S_{3p} (total)	0.75	0.71	0.91	1.08
S_{3p} (Sulfur 1)	0.75	0.71	0.54	0.53
S_{3p} (Sulfur 2)	-	-	0.37	0.27
S_{3p} (Sulfur 3)	-	-	-	0.27
O_{2p} (Oxygen 1)	0.14	0.12	0.07	-
O_{2p} (Oxygen 2)	0.14	0.12	-	-
ref.	26	26	this work	30

in spin density for SO_2^-, S_2O^-, and S_3^- are in agreement with a simple argument based on electron repulsion. The unpaired electron which occupies a highly antibonding 2b", orbital is repelled to the less electronegative sulfur atom by the concentration of electron charge in bonding orbitals near the more electronegative oxygen atom. It is expected, therefore, that the central sulfur atom would increase in spin density as one moves up the series from SO_2^- to S_3^-. By a similar argument one would predict that the replacement of an oxygen atom by sulfur in SO_2^- would result in a greater charge density but a smaller spin density on the remaining oxygen atom.

At considerable lower temperatures trapped electrons on the surface of MgO react with H_2S forming a paramagnetic ion which has been identified as $H_2S_2^-$. It has been suggested that the ion was H_2S^-; however, the sulfur -33 hyperfine data provides convincing evidence that the molecule contains two, nonequivalent sulfur atoms. The spin density of the unpaired electron was predominantly localized in the 3p orbitals of the two nonequivalent sulfur atoms of the $H_2S_2^-$ radical. Since the sulfur atom has low-lying 3d oribtals, the

energy levels for the 3p and 3d orbitals may be close; thus, in principle, either a σ_{3d} bonding orbital or a σ_{3p}^* antibonding orbital may accomodate the unpaired electron. Consideration for the occupancy of the unpaired electron in the two possible molecular oribtals has been given by Akasaka et al. (32) in their study of the radicals $R\text{-}CH_2\text{-}\ S\dot{-}S\text{-}CH_2\text{-}R$ obtained by γ irradiation of L-cystine dihydrochloride. Using their experimental g tensor they found an energy splitting between the ground and the first excited state which was much too large when an occupancy of the σ_{3d} orbital was assumed. Therefore, the unpaired electron probably occupies the σ_{3p}^* antibonding orbital.

The CNDO calculations have further confirmed that the d orbital contribution to the bonding in sulfur-containing molecules is relatively small. These calculations also provide one of the first attempts to determine the structure of adsorbed molecules by comparing calculated and experimental magnetic parameters. The approach is unique in that we attempt to minimize the differences between calculated and experimental parameters, in contrast to the usual method of estimating geometries whereby the total energy is minimized with respect to bond lengths and bond angles. The latter method suffers from the fact that the calculated minimum energies may not be directly compared with experimental values. Comparing the CNDO/2 - calculated g tensors with those reported by Chuvylkin and Zhidomorov (33) on the CO_2^- ion we found that our calculated values (2.0032, 1.9975, 2.0023) are much closer to the experimental values (2.0032, 1.9975, 2.0014) than theirs (2.0085, 1.9957, 2.0024). Moreover, the CNDO/2 calculation gives 121° as the best possible bond angle for the CO_2^- ion, which is very close to the 124° predicted from the sp hybridization as calculated from the hyperfine structure (34,35). The calculated bond angles from the EPR spectroscopic study were 115 ± 5° for the SO_2^- ion, according to Dinse and Möbius (36), and the CNDO/2 calculation indicates 120 and 110° for SO_2^- (A) and (B), respectively. More support for the accuracy of the CNDO/2 method comes from comparison with the scattered wave-SCF-Xα method, by which a bond length and bond angle of the S_3^- ion were calculated (37) to be 2.05-2.10Å and 110 ± 5°, respectively. The CNDO/2 method together with experimental g values indicates a best fit at 2.1Å and 110°. The bond lengths of the sulfur-containing anions are long by 0.1 to 0.3Å, compared to the neutral molecules. This may be due to the repulsion which arises from the extra electron.

SECTION 5

LIST OF PUBLICATIONS

1. "Electron Paramagnetic Resonance Evidence for the Formation of S_2O^- on Magnesium Oxide", M. J. Lin and J. H. Lunsford, J. Phys. Chem., 80, 635-639 (1976).

2. "An Electron Paramagnetic Resonance Study of the $H_2S_2^-$ Radical on Magnesium Oxide", M. J. Lin and J. H. Lunsford, J. Phys. Chem., 80, 2015-2018 (1976).

3. "Surface Reactions of SO_2 with NO_2 on Hydrated Silica Gel", S. M. Davis and J. H. Lunsford, J. Environ. Sci. Health, A11, 735-741 (1976).

4. "Low-Temperature Surface Oxidation of Hydrogen Sulfide by Oxygen", M. J. Lin and J. H. Lunsford, J. Environ. Sci. Health, A12, 127-136 (1977).

5. "CNDO Calculations of the g Tensors and Spin Densities of Small Paramagnetic Sulfur-Containing Anions on Magnesium Oxide", M. J. Lin and J. H. Lunsford, J. Magnetic Res., 29, 151-157 (1978).

6. "Surface Reactions of SO_2 with NO_2 on Hydrated Silica and Silica-Alumina", S. M. Davis and J. H. Lunsford, J. Colloid Interface Sci., 65, 352-364 (1978).

7. "The Oxidation of SO_2 with O_2 on MnY Zeolites", J. R. Pearce and J. H. Lunsford, J. Colloid Interface Sci., in press.

REFERENCES

1. Maurin, P. G., and J. Jonakin. Removing sulfur oxides from stacks. Chem. Eng. (New York), 77(9): 173-80, 1969.

2. Shy, C. M., and J. F. Finklea. Air pollution affects community health. Environ. Sci. Technol., 7:204-208, 1973.

3. Prince, R., and F. F. Rose. Sulfur in air and soil. Water, Air and Soil Pollut., 1:286-302, 1972.

4. Johnstone, H. F. Metallic ions as catalysts for the removal of sulfur dioxide from boiler furnace gases. Ind. Eng. Chem., 23:559-561, 1931.

5. Johnstone, H. F. and D. R. Coughanowr. Absorption of sulfur dioxide from air. Ind. Eng. Chem., 50:1169-1172, 1958.

6. Cheng. R. T., M. Corn and J. O. Frohliger. Contribution to the reaction kinetics of water soluble aerosols and SO_2 in air at ppm concentrations. Atmospheric Environment, 5:987-1008, 1971.

7. Renzetti, N. A., and G. J. Doyle. Photochemical aerosol formation in sulfur dioxide-hydrocarbon systems. Int. J. Air Pollut., 2:327-345, 1960.

8. Jaffe, S., and F. S. Klein. Photolysis of NO_2 in the presence of SO_2 at 3660A. Trans. Faraday Soc., 62:2150-7, 1966.

9. Bourbigot Y., J. Bricard, G. Madelaine, and D. Vigla. Identification of aerosols produced by photolysis in the presence of sulfur dioxide. C. R. Acad. Sci., 276:547-50, 1973.

10. Canosa, C., W. G. Filby, and R. D. Penzhorn. On the gas phase products from the thermal and photochemical nitrous oxide-sulfur oxide (SO_x) reaction. J. Environ. Sci. Health, Part A, A11(1):93-8, 1976.

11. Cook. W. G. and R. A. Ross, Heterogeneous oxidation of hydrogen sulfide at concentrations below 1000 ppm in nitrogen/air mixtures over supported metal oxide catalysts. Atmos. Environ., 7:145-51, 1973.

12. Steijns, M., and P. Mars. Role of sulfur trapped in micropores in the catalytic partial oxidation of hydrogen sulfide with oxygen. J. Catal., 35:11-17, 1974.

13. Steijns, M., F. Derks, A. Verloop and P. Mars. The mechanism of the catalytic oxidation of hydrogen sulfide. II. Kinetics and mechanism of hydrogen sulfide oxidation catalyzed by sulfur. J. Catal., 42:87-95, 1976.

14. Menon, P. G., R. Sreeramamurthy, and P. S. Murti. Experimental study of temperature and rate profiles in a rapidly fouling catalyst bed. Chem. Eng. Sci., 27:641-4, 1972.

15. Steijns, M., P. Koopman, B. Nieuwenhuijse, and P. Mars. The mechanism of the catalytic oxidation of hydrogen sulfide. III. An electron spin resonance study of the sulfur catalyzed oxidation of hydrogen sulfide. J. Catal., 42:96-106, 1976.

16. Belitskus, D. L. Oxidation of molten aluminum-magnesium alloy in air, air-sulfur dioxide, and air-hydrogen sulfide atmospheres. Oxid. Metals, 3:313-17, 1971.

17. Fischer, F., L. Goens, and H. Kraus. Reactions of hydrogen sulfide in sorption from oxygen-rich gases on activated carbon. Chem. Ingr. Tech., 36:963-8, 1964.

18. Pearce, J. R., and J. H. Lunsford. The oxidation of SO_2 with O_2 on MnY Zeolites. J. Colloid Interface Sci., in press.

19. Davis, S.M., and J. H. Lunsford. Surface reactions of SO_2 with NO_2 on hydrated silica gel. J. Environ. Sci. Health, A11:735-741, 1976.

20. Davis, S. M. and J. H. Lunsford. Surface reactions of SO_2 with NO_2 on hydrated silica and silica-alumina. J. Colloid Interface Sci., 65:352-364, 1978.

21. Lin, M. J., and J. H. Lunsford. Low-temperature surface oxidation of hydrogen sulfide by oxygen. J. Environ. Sci. Health, A12:127-136, 1977.

22. Lin, M. J., and J. H. Lunsford. An electron paramagnetic resonance study of the $H_2S_2^-$ radical on magnesium oxide. J. Phys. Chem. 80:2015-3018, 1976.

23. Lin, M. J., and J. H. Lunsford. Electron paramagnetic resonance evidence for the formation of S_2O^- on magnesium oxide. J. Phys. Chem., 80: 635-639, 1976.

24. Lin, M. J. and J. H. Lunsford. CNDO calculations of the g tensors and spin densities of small paramagnetic sulfur-containing anions on magnesium oxide. J. Magnetic Res., 29:151-157, 1978.

25. Morton, J. R. Identification of some sulfur-containing radicals trapped in single crystals. J. Phys. Chem., 71:89-92, 1967.

26. Schoonheydt, R. A., and J. H. Lunsford. Electron paramagnetic resonance of SO_2^- on magnesium oxide. J. Phys. Chem., 76:323-8, 1972.

27. Ono, Y., H. Tokunaga, and T. Keii. Electron spin resonance study of sulfur dioxide (I^-) radicals on synthetic zeolites. J. Phys. Chem. 79: 752-6, 1975.

28. Schneider, J., B. Dischler, and A. Raeuber. Electron spin resonance of sulfur and selenium radicals in alkali halides. Phys. Status Solidi, 13:141-57, 1966.

29. McLaughlin, S. D., and D. J. Marshall. Paramagnetic resonance of sulfur radicals in synthetic sodalites. J. Phys. Chem., 74:1359-63, 1970.

30. Lunsford, J. H., and D. P. Johnson. Electron paramagnetic resonance study of triatomic sulfur ion formed on magnesium oxide. J. Chem. Phys., 58:2079-83, 1973.

31. Bennett, J.E., B. Mile, and A. Thomas. Preparation and properties of the H_2S negative ion. Chem. Commun. 7:182-4, 1966.

32. Akasaka, K., S. Ohnishi, T. Suita, and I. Nitta. Electron spin resonance (E.S.R.) of a single crystal of L-cystine dihydrochloride irradiated at low temperature. J. Chem. Phys., 40:3110-16, 1964. Akasaka, K., S. Kominami, and H. Hatano. Photoinduced hole-electron recombination in a γ-irradiated single crystal of L-cystine dihydrochloride. J. Phys. Chem., 75:3746-50, 1971.

33. Chuvylkin, N. D., and G. M. Zhidomirov. Calculations of the anisotropic hyperfine coupling constants in free radicals. J. Magn. Resonance. 11: 367-72, 1973.

34. Meriaudeau, P., J. C. Vedrine, Y. Ben Taarit, and C. Naccache. Electron paramagnetic resonance studies of carbon dioxide anion radicals adsorbed on magnesium oxide. Identification and structure of the species using carbon-13 and oxygen-17 labeling. J. Chem. Soc. Faraday Trans. II, 71:736-48, 1975.

35. Lunsford, J. H. and J. P. Jayne. Formation of CO_2^- radical ions when CO_2 is adsorbed on irradiated magnesium oxide. J. Phys. Chem., 69:2182-4, 1965.

36. Dinse, K. P., and K. Moebius. E. P. R. studies of electrolytically generated SO_2 . Z. Naturforsch, 23:695-702, 1968.

37. Cotton, F. A., J. B. Harmon, and R. M. Hedges. Calculation of the ground state electronic structures and electronic spectra of di- and trisulfide radical anions by the scattered wave SCF-Xα method. J. Am. Chem. Soc., 98:1417-24, 1976.

TECHNICAL REPORT DATA
(Please read Instructions on the reverse before completing)

1. REPORT NO. EPA-600/7-79-088	2.	3. RECIPIENT'S ACCESSION NO.
4. TITLE AND SUBTITLE SURFACE REACTIONS OF OXIDES OF SULFUR		5. REPORT DATE April 1979
		6. PERFORMING ORGANIZATION CODE
7. AUTHOR(S) J.H. Lunsford		8. PERFORMING ORGANIZATION REPORT NO.
9. PERFORMING ORGANIZATION NAME AND ADDRESS Department of Chemistry, Texas A&M University, College Station, Texas 77843		10. PROGRAM ELEMENT NO. 1NE625 (EA 21) FY77
		11. CONTRACT/GRANT NO. 801136
12. SPONSORING AGENCY NAME AND ADDRESS Environmental Sciences Research Laboratory - RTP, NC, Office of Research and Development, U.S. Environmental Protection Agency, Research Triangle Park, North Carolina 27711		13. TYPE OF REPORT AND PERIOD COVERED Final 12/73 to 5/78
		14. SPONSORING AGENCY CODE EPA/600/09

15. SUPPLEMENTARY NOTES

16. ABSTRACT

Surface reactions of several sulfur-containing molecules have been studied in order to understand the mechanism by which sulfate ions are formed on atmospheric aerosols. At 25°C the heterogeneous oxidation of SO_2 by NO_2 to sulfuric acid and sulfate ions occurred on hydrated silica and silica-alumina surfaces. The oxidation of SO_2 by O_2 was undetectably slow on these surfaces; however, the reaction was catalyzed by Mn^{2+} ions in a Y-type zeolite. In this case the only reaction product was a SO_4^{2-} species which was strongly bound in the zeolite micropores. Molecular oxygen also reacted with H_2S on zeolites and magnesium oxide. The primary reactions on zeolites resulted in the formation of elemental sulfur; whereas, on MgO a variety of products were observed including elemental sulfur, sulfide ions, sulfite ions and a number of paramagnetic ions such as S_3^-, S_2O^- and S_n^-. Experiments were also carried out to identify and to determine the mechanism by which S_2O^- and $H_2S_2^-$ are formed on MgO. To establish the geometric structure of the S_2O^- ion and other paramagnetic sulfur-containing molecules on MgO, CNDO semiempirical calculations were carried out to determine theoretical values of g tensors and spin densities as a function of bond angles and bond lengths.

17. KEY WORDS AND DOCUMENT ANALYSIS

a. DESCRIPTORS	b. IDENTIFIERS/OPEN ENDED TERMS	c. COSATI Field/Group
*Air pollution *Sulfur oxides *Chemical reactions *Aerosols *Surface chemistry *Ion exchange resins		13B 07B 07D

18. DISTRIBUTION STATEMENT RELEASE TO PUBLIC	19. SECURITY CLASS (This Report) UNCLASSIFIED	21. NO. OF PAGES 42
	20. SECURITY CLASS (This page) UNCLASSIFIED	22. PRICE

EPA Form 2220-1 (9-73)